water

MDPI

Article

Hydrochemical Characteristics and Thermal Reservoir Temperature Estimation of a Fault-Controlled Geothermal Field in the Northern Qinghai Lake Coalfield Area

Yongxing Zhang [1,2], Zexue Qi [2,*], Bin Ran [3], Sheng He [2], Jingrong Zhao [2], Hengheng Wang [2] and Wenlong Pang [2]

[1] College of Earth and Environmental Sciences, Lanzhou University, Lanzhou 730000, China
[2] Xining Center of Natural Resources Comprehensive Survey, China Geological Survey, Xining 810021, China
[3] School of Water and Environment, Chang'an University, Xi'an 710054, China
* Correspondence: qzx13639722055@126.com

Abstract

This study explores the hydrochemical and thermal characteristics of a fault-controlled geothermal field within the Northern Qinghai Lake Coalfield Area on the northeastern Qinghai–Tibetan Plateau (QTP). This research integrates hydrochemical analyses, isotopic tracers, and the regional geological framework to define hydrochemical signatures, identify recharge sources and flow paths, assess cold–hot water mixing, estimate reservoir temperatures, determine circulation depths and residence times, and explain the geothermal system's formation. Systematic sampling included geothermal waters, cold springs, and surface waters, followed by laboratory analysis of major ions, stable isotopes (δ^2H, δ^{18}O), radiocarbon (^{14}C), and tritium (^{3}H). The geothermal water is categorized as a low-temperature, weakly acidic to near-neutral HCO_3-Ca•Mg type, exhibiting temperatures from 35.6 to 46.2 °C. Isotopic analyses indicate that cold spring and river waters align with the local meteoric water line, while geothermal waters display distinct isotopic signatures, suggesting deeper circulation. A silica–enthalpy mixing model reveals substantial cold-water mixing during upwelling, with mixing ratios between 74.5% and 85.6%. The corrected recharge elevation is estimated to be 4378–4456 amsl, implying a primary recharge zone in the branch of the Qilian mountains—the middle section of Datong Mountain to the northeast. Geothermometry, employing quartz and chalcedony temperature scales and accounting for mixing, estimates reservoir temperatures of 150–202 °C. The calculated circulation depth spans 3211–4291 amsl. Low tritium levels and carbon dating suggest a deep-cycling system predating 1952, characterized by deeply circulating "ancient water". The geothermal system's development is associated with regional tectonics, fault systems, and the Kesuer Formation (J_xk) acting as the reservoir. This study provides a scientific foundation for the development and sustainable use of geothermal resources in the northern Qinghai Lake region and offers insights applicable to comparable fault-controlled geothermal systems across the QTP.

Keywords: geothermal fluids; hydrochemical; thermal reservoir temperature; genetic mechanism

Check for updates

Academic Editor: Paula M. Carreira

Received: 3 November 2025
Revised: 30 December 2025
Accepted: 7 January 2026
Published: 27 February 2026

Copyright: © 2026 by the authors. Licensee MDPI, Basel, Switzerland. This article is an open access article distributed under the terms and conditions of the Creative Commons Attribution (CC BY) license.

1. Introduction

Geothermal energy, characterized by low emissions, renewability, and the potential for both direct use and power generation, is increasingly recognized as a strategic clean energy resource in the context of the energy transition and rising energy demand [1]. Among

regions with significant geothermal potential, the Qinghai–Tibetan Plateau (QTP) hosts abundant and diverse geothermal systems [2], notably fault-controlled (fracture-type) and basin-type systems. Fault-related permeability, high heat flow, and active tectonism together create favorable conditions for the formation and circulation of geothermal fluids [3] across the QTP.

Over the past decade, substantial progress has been made in clarifying the occurrence patterns and conceptual models of QTP geothermal systems [4]. For example, ion-correlation analyses have been used to identify mixing between cold and thermal waters in the Guide Basin and to estimate reservoir temperatures through geochemical geothermometry [5]. Studies in the Xining geothermal field have highlighted the role of controlling faults and integrated hydrochemical and isotopic evidence to propose preliminary regional conceptual models. Yuan et al. [6] analyzed spatial patterns of seismicity and geothermal manifestations in Qinghai Province and further explored links between earthquake intensity and geothermal development [7]. In the Gonghe Basin, the heat-source mechanism and fluid aggregation have been investigated by combining isotope geochemistry, hydrochemistry, and geophysical exploration [8]. Work in the Reshuiquan area of Guide and in Yangbajing (Tibet) underscores that geothermal circulation is primarily channeled along fracture zones, with deep heat storage associated with slip-fault systems within metamorphic bedrock—typical of fractured bedrock (fissure-type) reservoirs [9].

The northeastern margin of the Tibetan Plateau is a significant geothermal anomaly zone in China, characterized by terrestrial heat flow values substantially higher than the global average. Taking the adjacent Gonghe Basin as an example, the measured average terrestrial heat flow reaches 90.56 ± 22.18 mW/m^2, classifying it as a typical high heat flow basin, with its heat flow distribution exhibiting higher values in the northeast and lower values in the west [10]. Geophysical exploration has revealed the widespread presence of a low-velocity and high-conductivity layer in the mid-lower crust of this region, commonly interpreted as a partial-melt body, which serves as a crucial intra-crustal heat source [10,11]. Concurrently, the area exhibits a typical "hot crust and cold mantle" thermal structure, meaning that the surface heat flow primarily originates from the crustal contribution [12,13]. For instance, studies indicate that the crust-to-mantle heat flow ratios in regions such as Qilian, Tongren, Xunhua, and Menyuan are all greater than 1 (e.g., approximately 1.78:1 in the Qilian area), confirming that heat generation from crustal radioactive elements and intra-crustal partial melting are the dominant heat sources. Driven by regional tectonic forces, deep thermal energy is transported upwards through mechanisms such as lower crustal channel flow and deep major fault systems (e.g., the Wenquan–Wahong Mountain Fault and the Riyue Mountain Fault) [10,14], ultimately accumulating within suitable reservoir–cap combinations to form geothermal resources. This regional geothermal framework provides a key context for understanding the heat source mechanism of the Northern Qinghai Lake Coalfield Area.

Despite these advances, the hydrochemical characteristics and genesis of fault-controlled geothermal waters in the coalfield area north of Qinghai Lake remain insufficiently constrained [15]. To date, this area has only been analyzed with basic geological–hydrological surveys focused on coal resources, with no comprehensive, integrated assessment of its geothermal potential. Addressing this gap is important for regional resource evaluation and for refining the broader understanding of fracture-type geothermal systems on the QTP.

This study investigates the geothermal water system in the vicinity of the coalfield north of Qinghai Lake. We conduct systematic sampling of geothermal waters, cold springs, and surface waters within the relevant aquifers and integrate these data with the regional geological framework. Using hydrochemical analyses and isotopic constraints,

we (i) characterize the hydrochemical signatures and dominant water–rock interaction processes; (ii) identify recharge sources and flow paths; (iii) evaluate cold–hot water mixing; (iv) estimate reservoir temperatures using geothermometric approaches; (v) infer circulation depths and residence times (ages); and (vi) elucidate the formation mechanism and develop a conceptual model of the geothermal system. The results provide a scientific basis for the development and sustainable utilization of geothermal resources in the northern Qinghai Lake area and offer insights applicable to analogous fault-controlled geothermal systems across the QTP.

2. Materials and Methods

2.1. Geographical Location and Climate Environment

The research site is located in the northeastern QTP (Figure 1a), approximately 50 km north of Qinghai Lake (Figure 1b). It is readily accessible via a provincial highway that traverses the site from the southeast to the northwest. The area extends from 100°19′58″ to 100°22′37″ E, and 37°39′39″ to 37°41′01″ N, covering roughly 10 km^2. Topographically, the landscape is dominated by valley plains at an average elevation of about 3650 m. Spurs of Datong Mountain are present to the northwest and northeast, forming a medium-high mountainous terrain shaped by erosional processes. The overall relief is higher in the north and lower in the south, with gentle regional slopes of approximately 2–5°.

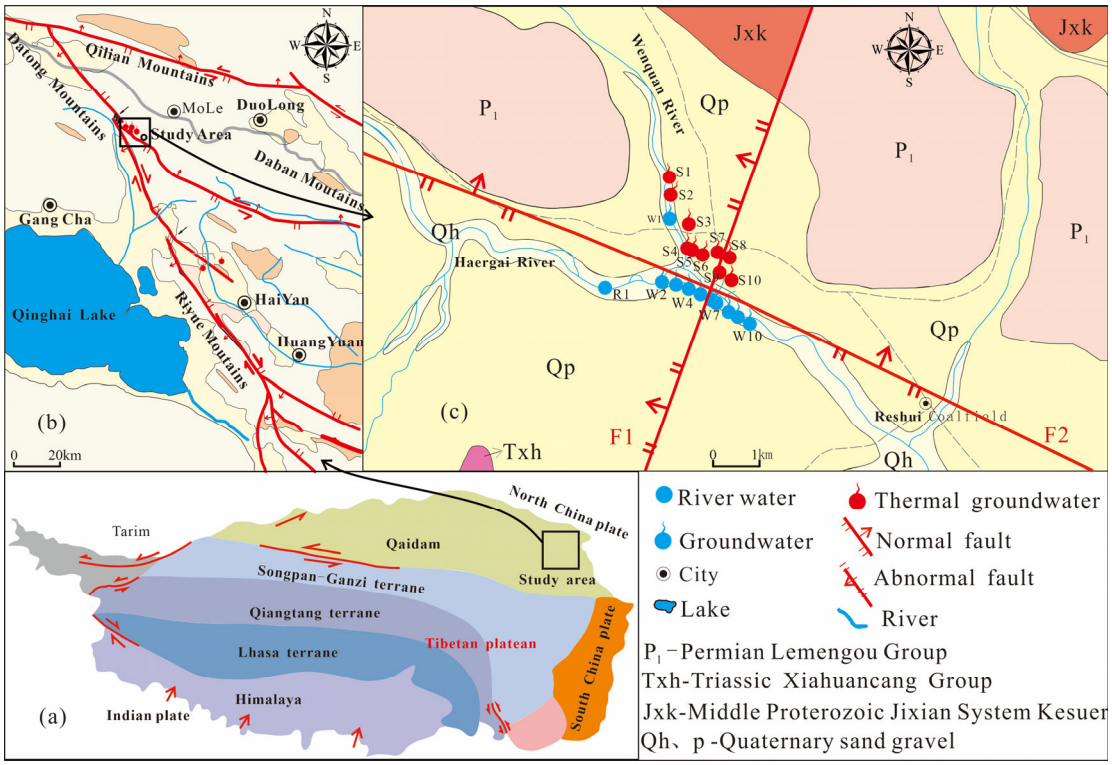

Figure 1. Map of (**a**) the tectonic setting of the Tibetan Plateau, (**b**) the geological setting of the eastern Qinghai Lake basin, and (**c**) the geology and distribution of sampling points in the study area.

The region has a semi-arid plateau continental climate and is influenced by the intersection of the mid-latitude westerlies, South Asian monsoons, and East Asian monsoons. Local microclimatic effects from Qinghai Lake further increase climatic variability. The mean annual air temperature is 0.5 °C. The mean annual precipitation is 393.62 mm, while the mean annual potential evaporation is approximately 1440.16 mm. The average annual relative humidity is 54.8%. Precipitation increases with elevation, whereas evaporation displays an inverse relationship.

Surface drainage is limited and consists primarily of small thermal-spring gullies and the headwaters of the Hargai River (Figure 1c). Groundwater recharge is mainly derived from meteoric precipitation and seasonal melting of mountain snow and ice. Owing to low population density, anthropogenic contamination is minimal. The surrounding bedrock locally contains trace elements that may be detectable in the thermal–mineral waters.

Thermal springs are concentrated near the hot-spring gully that flows toward the Hargai River, chiefly within the river's floodplain and first terrace. Within the ~10 km^2 area, more than 10 major spring outlets are mapped (Figure 1c). Among these, 12 individual vents discharge at approximately 0.5 L/s, five vents exceed 0.5 L/s, and two vents exceed 1 L/s. Based on incomplete measurements, the cumulative discharge is greater than 9.01 L/s (778 m^3/d). Measured spring temperatures range from 35.6 to 46.2 °C. The spring group is currently undeveloped and remains in a natural state.

2.2. Geological and Hydrogeological Conditions

Following the tectonic unit division of the Chinese mainland and based on the 1:1,000,000 geological map of Qinghai Province [16] and analyses of the tectonic evolution of the Qilian Mountains [17], the study area is assigned to the early Paleozoic Qin–Qi–Kun orogenic belt, which is within the broader orogenic system of the Qilian Mountains. Faults in the area are diverse. Style-reverse, strike-slip, and normal faults of indeterminate kinematics exert first-order control on the distribution and juxtaposition of stratigraphic units. Multiple formations are dissected by faults of differing orientations, partitioning the bedrock into blocks of variable sizes.

In the Middle Qilian region, a suite of ductile faults formed within the Proterozoic strata and was later overprinted by late-stage structures. The latter are predominantly brittle overthrust faults that developed mainly during the late Mesozoic and subsequently influenced the Cenozoic stratigraphic architecture and structural fabric. A branch of the Reshui–Riyueshan fault system is the most significant structure within the study area. This fault trends approximately 125°, dips steeply to the southwest, and is mapped as a reverse fault (F2) (Figure 1c). It records a transition from ductile behavior to brittle behavior, with reactivation in Mesozoic time within early Paleozoic rocks. In addition, northeast-trending extensional (tension) faults (F1) are present locally. Together, NW-SE to WNW-ESE compressional–shear faults and NE-trending extensional segments form conjugate sets that enhance fracture permeability and control fluid pathways.

The principal stratigraphic units include the following: (1) Jixian System, Kesuer Formation (Jxk): It has relatively stable to sub-stable carbonate successions interbedded with shallowly metamorphosed fine clastic rocks. Lithologies include silty slate interbedded with sandstone, dolomite, and crystalline limestone. (2) Permian, Lemengou Formation (P1): It has purplish-red to gray-green feldspathic quartz sandstone, along with quartz sandstone and gray sandstone containing siltstone. The lower part locally contains a fine quartzose conglomerate. (3) Triassic, Lower Huancang Formation (Txh): It contains gray-white fine gravelly quartz sandstone in the lower region, along with local feldspathic quartz sandstone at the base. The upper part comprises light gray, medium-grained quartz sandstone bearing bivalve fossils. (4) Quaternary Deposits (Qh and Qp): They consist of valley and gully fills dominated by sand, gravel, and pebbles.

Based on lithologic controls and relative water abundance, groundwater in the study area can be classified into three types: (1) Porous aquifers in unconsolidated deposits (Hargai River valley): The aquifer is composed of sand–gravel layers with a thickness of approximately 10–15 m. The depth to water ranges from about 1 to 10 m. Hydrochemistry is dominated by HCO_3–Ca·Mg facies. (2) Water above frozen bedrock layers in mountainous terrain (suprapermafrost groundwater): This type is chiefly distributed at elevations of

3800–4200 m, where intensely weathered bedrock is pervasively fractured. Abundant perched water accumulates above frozen layers, producing numerous springs with typical discharges of 8–12 L/s. Total dissolved solids are generally less than 0.2 g/L, and the predominant hydrochemical type is HCO_3–Ca. (3) Fracture-zone (vein-like) water along fault zones: These occur where faults are well developed, particularly along NW–W-trending compressional–shear faults and in the composite zones where NE-trending tensile (F1) segments intersect or abut reverse faults (F2). Springs are concentrated in the hanging-wall damage zones of compressional–shear faults and in the overlap of tensile structures. Typical spring discharges range from 1 to 5 L/s.

2.3. Field Survey and Sampling

In June 2022, a geothermal geological survey and a water sampling campaign were conducted in the study area. A total of 21 water samples were collected for hydrochemical and isotopic analyses, including 10 geothermal spring samples (S1–S10) and 10 cold spring samples (Q1–Q10) from the hot-spring gully and the Hargai River floodplain. Sampling locations are shown in Figure 1c. Before collection, high-density polyethylene (HDPE) bottles were rinsed thoroughly with the target sample water. Samples were sealed, labeled, stored at 4 °C, and transported to the laboratory within 48 h. In situ measurements of water temperature, pH, and electrical conductivity (EC) were obtained using a portable multiparameter meter (HANNA HI98130, Padua, Italy). Visual observations (color, odor, and visible particulates) were recorded at each site.

2.4. Laboratory Analyses and the Principle of Radioisotope Dating

All chemical and isotopic analyses were carried out at the Laboratory of Groundwater Science and Engineering, Institute of Hydrogeology and Environmental Geology, Chinese Academy of Geological Sciences. Major cations (K^+, Na^+, Ca^{2+}, and Mg^{2+}) were quantified by inductively coupled plasma mass spectrometry (ICP-MS; Agilent 7500ce, Tokyo, Japan). Major anions (SO_4^{2-}, Cl^-) were determined by ion chromatography (Shimadzu LC-10ADvp, Kyoto, Japan). Total dissolved solids (TDSs) were measured gravimetrically. Bicarbonate (HCO_3^-) was analyzed by acid–base titration. Stable isotopes of hydrogen and oxygen (δ^2H, $\delta^{18}O$) were measured using a liquid water isotope analyzer (LGR-DLT-100; Los Gatos Research, San Jose, CA, USA). Results are reported in delta (δ) notation relative to Vienna Standard Mean Ocean Water (VSMOW). Analytical precision is ±0.1‰ for δ^2H and ±0.01‰ for $\delta^{18}O$. Tritium (^3H) was determined by low-background liquid scintillation counting following 50-fold preconcentration of the water sample. Ion-charge-balance errors for all samples were within ±5%, indicating acceptable analytical accuracy and internal consistency across the dataset. ^3H as tritiated water, in combination with its stable daughter product ^3He, is generally considered to be one of the most reliable tracers for estimating the apparent age of post-1950 groundwater [18]. Radiocarbon (^{14}C) was analyzed by accelerator mass spectrometry (AMS) at Beta Analytical Inc. (Miami, FL, USA), and results are expressed as percent modern carbon (pMC) with measurement uncertainty < 0.1 pMC. The ^{14}C age value was determined based on Ref. [19].

$$t_0 = \frac{5730}{\ln 2} \ln \frac{A_{nd}}{A_{obs}} \quad (1)$$

where t_0 is the age of the ^{14}C in groundwater (pMC), while A_{obs} represents the measured ^{14}C values of groundwater samples. A series of models [19] (original data, mass balance, Vogel, Tamers, Mook, and Fontes & Garnier) were used to compute A_{nd}.

2.5. Silica–Enthalpy Mixing Model

In this study, the determination of the reservoir temperature of the initial geothermal water in the study area was achieved through the utilization of the silicon enthalpy equation. The fundamental premise of this method is the hypothesis that the initial geothermal water is amalgamated with cold surface water, thereby forming a hot spring [20].

$$H_c X + H_h(1 - X) = H_s \quad (2)$$

$$Si_c X + Si_h(1 - X) = Si_s \quad (3)$$

where X is the cold-water mixing ratio; H_c, H_h, and H_s are the enthalpy of surface cold water, the enthalpy of deep geothermal water, and the enthalpy of hot-spring water; and Si_c, Si_h, and Si_s are the SiO_2 content of surface cold water, the SiO_2 content of deep geothermal water, and the SiO_2 content of hot-spring water, respectively. For temperatures above 100 °C, the relationship between temperature and the enthalpy of saturated water can be found in Table 1 [21].

Table 1. The relationship between the temperature of hot water, enthalpy, and SiO_2.

Temperature, °C	Enthalpy, J/g	SiO_2, mg/L
100	100.1	48.0
125	125.1	80.0
150	151.0	125.0
175	177.0	185.0
200	203.6	265.0
225	230.9	365.0
250	259.2	486.0
275	289.0	614.0
300	321.0	692.0

2.6. Recharge Elevation Estimation from Stable Isotopes

The stable isotopic composition of meteoric waters (δ^2H and $\delta^{18}O$) becomes progressively depleted with increasing elevation (altitude effect). Accordingly, groundwater δ-values largely reflect the elevation of recharge when evaporative enrichment prior to infiltration is negligible, and post-infiltration processes do not fractionate H and O isotopes [22]. Recharge elevation can be estimated from the measured isotopic composition of springs or wells using an empirically derived isotope–elevation gradient for local precipitation [23].

$$H_R = 100 \times \frac{\delta D_s - \delta D_p}{K} + H_0 \quad (4)$$

where H_R is the recharge elevation (m) of the geothermal water source area; H_0 is the elevation (m) of the sampling site; δD_s and δD_p represent the δD values for water sampling points and atmospheric precipitation, respectively ($\delta Dp = -55.4‰$ [24]); and K is the δD elevation gradient value for atmospheric precipitation (−0.18‰/100 m) [24].

Geothermal discharge in the study area undergoes dilution during upwelling due to entrainment of shallow-circulation cold water, which modifies the hydrogen and oxygen isotopic composition of the mixed outflow. To estimate the deep geothermal end-member and quantify the impact of cold-water mixing, we adopt a conservative binary mixing formulation for δD [25].

$$\delta D_A = \frac{\delta D_C - f \times \delta D_B}{1 - f} \quad (5)$$

where δD_A denotes the final deuterium isotopic composition of the original hot water; δD_B represents the measured final deuterium isotopic composition of the original cold water; δD_C signifies the measured deuterium isotope value of geothermal water after admixture with cold water; and f denotes the mixing ratio of cold water.

2.7. Correction of Mixing Bias in Silica Geothermometry

Because discharge temperatures are below the local boiling point and field observations indicate no steam separation, we applied the no-steam-loss silica geothermometers for quartz and chalcedony to estimate reservoir (heat-storage) temperatures using the mixing-corrected SiO_2 concentration of spring water [23]. The calibrations used were as follows:

$$T = \frac{1309}{5.19 - \lg(SiO_2)} - 273.15 \quad (6)$$

$$T = \frac{1032}{4.6 - \lg(SiO_2)} - 273.15 \quad (7)$$

2.8. Estimation of Geothermal Water Circulation Depth

To estimate the circulation depth of geothermal waters in the hydrothermal area, we adopt the following relation [26]:

$$H = \mathrm{h} + \frac{t_1 - t_0}{c} \quad (8)$$

where H denotes the depth of geothermal water circulation (m); h is the thickness of the constant temperature zone (m), which is set at 30 m [27]; t_1 signifies the heat storage temperature (°C); t_0 indicates the local average annual temperature, which is −2.4 °C; and c stands for the geothermal gradient and is assumed to be 4.8 °C/100 m [27].

3. Results and Discussion

3.1. Hydrogeochemical Characteristics

The hydrogeochemical characteristics of surface water and groundwater (spring water) in the study area are presented in Table 2. Surface river water exhibits a pH of 7.51 and a temperature of 10.3 °C. In comparison, geothermal water shows a pH range of 6.42 to 7.00, with an average of 6.66, and temperatures ranging from 23.3 to 46.2 °C, averaging 37.2 °C. Total dissolved solids (TDSs) in geothermal water vary between 833.3 and 1614 mg/L, with an average of 1058 mg/L. Over twenty geothermal springs emerge at the surface, forming a spring group. The dominant cations, in order of abundance, are Ca^{2+}, Mg^{2+}, Na^+, and K^+, while the primary anions, in decreasing order, are HCO_3^-, SO_4^{2-}, and Cl^-. Free CO_2 concentrations vary between 91.99 and 602.7 mg/L, with an average of 193.7 mg/L.

Most spring points exhibit concentrations and temperatures that exceed medical thresholds for free carbon dioxide levels and total dissolved solids (TDSs), further confirming their classification as low-temperature weakly acidic geothermal water. These characteristics suggest significant potential for therapeutic applications, making these springs a valuable resource for both scientific study and potential utilization in the health and wellness industry. Moreover, the hydrogeochemical compositions of surface water

and groundwater (spring water) in the study area are detailed in Table 2, providing a comprehensive understanding of the region's hydrological dynamics. This data is essential for further research and sustainable management of these geothermal resources.

Table 2. Physical properties and hydrochemical compositions of water samples in the study area.

Sample NO.	Temperature (°C)	pH	TDS	CO_2	K^+	Na^+	Ca^{2+}	Mg^{2+}	Cl^-	SO_4^{2-}	HCO_3^-
			mg/L								
S1	35.90 *	7.00	939.2	131.8	14.60	44.7	176.4	92.34	28.36	91.26	982.4
S2	46.20 *	6.92	1614 *	212.0	23.80	254.9	218.4	69.26	28.36	509.1	1019
S3	35.90 *	6.73	1045 *	123.8	23.60	70.80	216.4	64.40	24.82	144.1	1001
S4	35.60 *	6.73	918.1	133.5	23.70	35.20	216.4	66.83	24.82	50.43	1001
S5	42.80 *	6.47	833.3	176.8	22.30	32.65	188.5	64.40	24.82	45.63	909.2
S6	44.60 *	6.5	981.6	272.6 *	25.91	41.80	195.2	76.06	42.54	102.8	951.9
S7	43.80 *	6.61	969.8	236.5	26.62	44.24	184.4	86.27	45.38	102.78	939.7
S8	43.60 *	6.42	993.5	159	27.07	45.04	198.4	80.19	44.67	104.71	964.1
S9	38.90 *	6.61	1024 *	602.7 #	26.200	43.40	195.2	77.27	46.09	103.26	994.6
S10	40.60 *	6.59	1442 *	212.0	21.34	44.95	191.6	70.55	21.43	92.47	943.5
W1	17.20	6.62	901.1	258.3 *	14.6	31.00	182.4	88.70	28.36	67.24	976.3
W2	18.40	6.31	1037 *	344.2 *	5.19	30.19	204.4	80.19	45.38	75.89	1031
W3	16.70	6.26	1040 *	260.7 *	21.86	36.35	202.0	79.22	47.50	72.05	1007
W4	17.90	6.58	484.9	423.9 *	11.39	35.41	88.18	35.24	36.87	60.52	402.7
W5	11.00	6.37	1027 *	259.9 *	21.41	36.64	202.4	77.76	46.09	72.05	994.6
W6	23.30	6.7	1014 *	170.8	23.80	59.80	212.4	71.69	21.27	120.08	1007
W7	30.70	6.77	1020 *	91.99	23.50	64.30	218.4	69.26	28.36	100.86	1031
W8	32.60	7.07	939.9	99.6	23.80	38.60	214.4	69.25	24.82	67.24	1001
W9	31.20	6.79	1134 *	131.4	24.20	101.2	212.4	70.47	28.36	184.44	1025
W10	31.70	6.95	1006 *	150.5	24.80	67.10	204.4	72.90	24.82	105.67	1013
R1	10.30	7.51	328.4	/	0.1	18.90	76.15	20.65	17.73	52.83	280.7

Notes: * indicates that the ion content meets the standard of natural mineral water for physiotherapy, while # indicates that the ion content has a concentration with medical value.

Most hot-spring waters meet the TDS levels for the drinking standards of natural mineral water, while some also comply with the therapeutic standards for natural mineral water, which are based on temperature and free CO_2 content. Cold spring water primarily originates from groundwater influenced by the intrusion of quaternary subsurface water or river water. The main chemical characteristics of these cold springs are as follows: pH values range from 6.26 to 6.62, with an average of 6.43; water temperatures range from 11 to 18.4 °C, averaging 16.24 °C; total dissolved solids (TDSs) range from 484.9 to 1040 mg/L, with an average of 897.94 mg/L. Cold spring water mainly emerges near the surface of river floodplains, displaying a cation pattern of $Ca^{2+} > Mg^{2+} > Na^+ > K^+$ and an anion pattern of $HCO_3^- > SO_4^{2-} > Cl^-$. The content of dissolved silicon dioxide averages 29.64 mg/L, ranging from 24.31 to 49.78 mg/L; dissolved carbon dioxide averages 309.4 mg/L, ranging from 258.3 to 423.9 mg/L. The levels of dissolved carbon dioxide and TDS in cold spring water meet natural mineral drinking standards, and their natural soda-water taste makes them promising candidates for developing high-quality composite natural mineral waters for drinking.

Upon comparing the ionic compositions of hot and cold spring waters (Table 2 and Figure 2), it is evident that the cation composition of the local geothermal water shares similarities with that of the cold spring water, with Ca^{2+} being the predominant ion in both. This suggests that both the host rock layers for the hot and cold waters are dominated by Ca^{2+}-rich strata, which undergo water–rock interactions, leading to the dissolution of Ca^{2+}-rich solutes. This observation is consistent with the high Ca^{2+} content found in carbonate rocks of the Jixian Series in this region. Additionally, both the local geothermal

water and cold spring water exhibit similar anion compositions, with HCO_3^- being the dominant ion. This is attributed to the dissolution of carbonate rocks by deep-seated, high-temperature water, which releases significant amounts of CO_2 gas, thereby increasing the prevalence of HCO_3^- in the groundwater. These findings are supported by the elevated CO_2 gas levels observed in the tested spring waters.

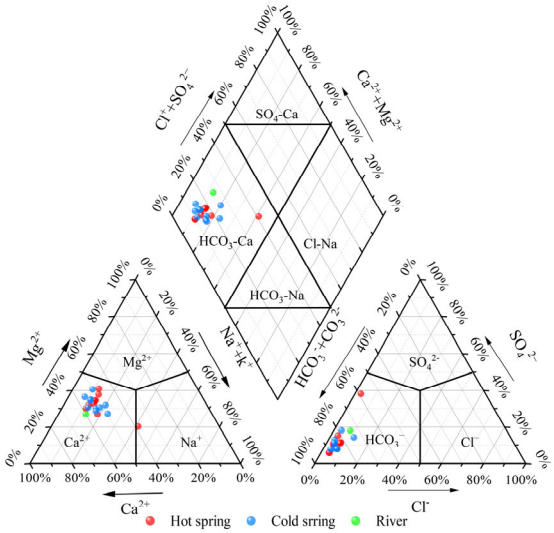

Figure 2. Piper diagram of water samples in the study area.

3.2. Characteristics of Environmental Isotope Composition

To comprehensively obtain environmental isotope information for cold springs and geothermal waters in the study area, an analysis of stable hydrogen and oxygen isotopes in cold spring water, geothermal water, and river water was conducted. These values were then compared with the local meteoric water line (LMWL) of the Qinghai Lake Basin, which is defined by the equation $\delta D = 8.69\delta^{18}O + 17.5$ [28].

As shown in Figure 3, the stable hydrogen and oxygen isotopes of the cold spring and river water in the research area predominantly align with the LMWL of the Qinghai Lake Basin, indicating their origin as meteoric water. In contrast, the geothermal water exhibits distinct isotopic characteristics. The δD and $\delta^{18}O$ values for the cold-water region range from −64.64‰ to −56.37‰ and −9.66‰ to −8.5‰, respectively, with average values of −60.12‰ for δD and −9.15‰ for $\delta^{18}O$. In the hot–cold-water transition zone, the δD values range from −61.74‰ to −64.93‰ (average: 63.09‰), and the $\delta^{18}O$ values range from −9.84‰ to −10.13‰ (average: −9.98‰). For the hot-water region, the δD values range from −64.35‰ to −65.34‰ (average: −64.82‰), and the $\delta^{18}O$ values range from −10.77‰ to −11.02‰ (average: −10.85‰). A gradual depletion of stable hydrogen and oxygen isotopes is observed from the cold-water region to the transition zone and then to the hot-water region.

The results indicate an interaction process between the geothermal water and oxygen-bearing carbonate minerals within the aquifer. Typically, due to evaporation, the $\delta^{18}O$ and δD values in geothermal water are more enriched compared to those in cold water. However, as shown in Figure 3, the geothermal water interacts with carbonate minerals that have a depleted ^{18}O signature, leading to a depletion of ^{18}O in the geothermal water itself. During the ascending process, the geothermal water mixes with cold water that has infiltrated from the surface and carries a more enriched ^{18}O signature, resulting in an intermediate $\delta^{18}O$ value in the mixed water.

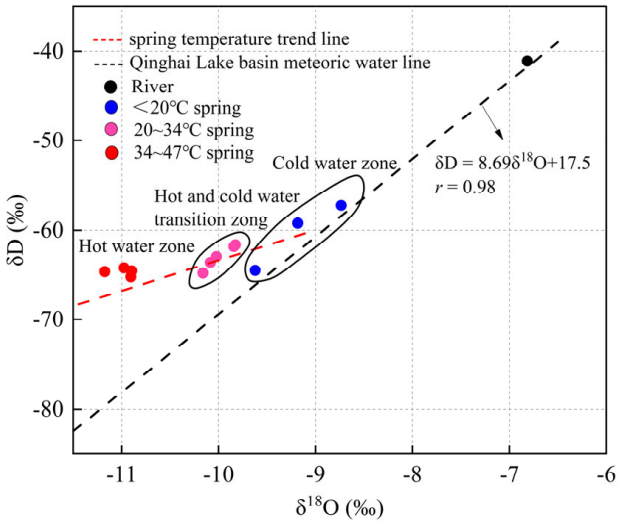

Figure 3. Distribution characteristics of $\delta^{18}O$ and δD in the study area.

3.3. Mixing of Hot and Cold Waters

Tectonic activities in hydrothermal areas are characterized by intense dynamics, resulting in the development of well-defined bedrock fractures and a complex network of river valleys. These geological conditions facilitate the emergence process by enabling the mixing of deep-circulating hot water with shallow-circulating cold water. As shown in Figure 3, the stable hydrogen and oxygen isotope composition of the various water bodies illustrates a progressive transition from cold water to hot water across the region. This isotopic gradient reflects the degree of mixing between cold and hot waters during the emergence of geothermal water.

Figure 4 illustrates the mixing ratios between hot and cold waters in the study area. The figure shows that a significant proportion of cold-water mixing occurs near the shallow surfaces during upwelling processes, with mixing ratios ranging from 74.5% to 85.6%.

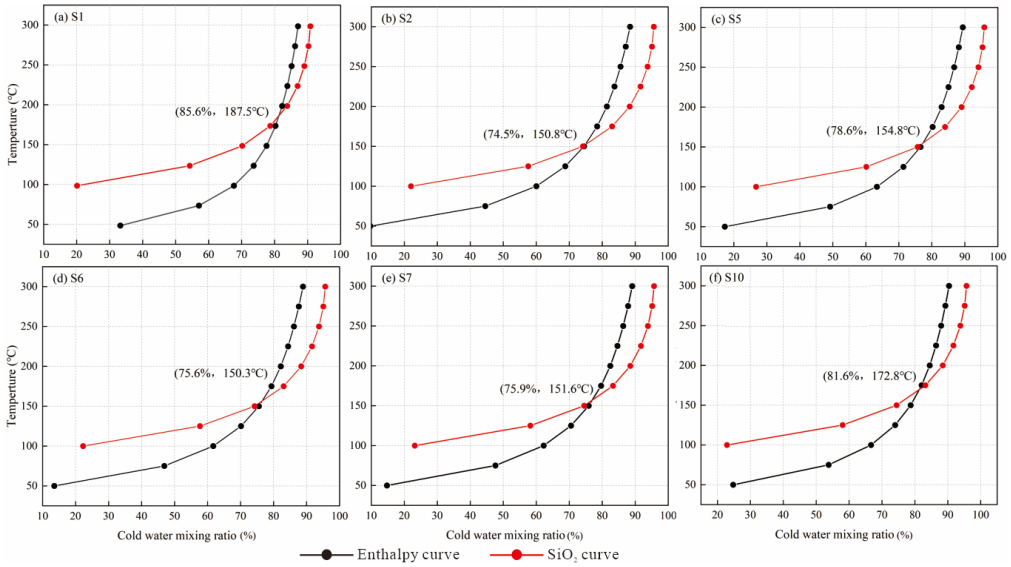

Figure 4. Relationship between the mixing ratio of hot water and cold water in groundwater. S1, S2, S5, S6, S7, and S10 represent the hot-spring sampling points.

3.4. Sources of Geothermal Water Supply

Stable isotopes of hydrogen and oxygen in water bodies are widely used as natural tracers to delineate the origin of groundwater recharge, runoff pathways, and the characteristics of recharge and drainage [29]. As illustrated in Figure 3, the discernible differences in hydrogen and oxygen isotopes between hot water and cold water in thermal areas indicate distinct recharge characteristics. Compared to cold water, the relative isotopic depletion observed in hot water suggests a higher recharge elevation. Furthermore, the notable drift in oxygen-18 values in hot water implies that underground thermal waters have undergone prolonged deep circulation after recharge, with oxygen isotopic exchange occurring between the thermal water and the surrounding rock matrix. The δD values of the hot-water mixture, determined using a binary mixing model, are presented in Table 3.

Table 3. Geothermal water supply elevation. $H_{R\text{-}A}$ and $HR\text{-}_C$ are the estimated recharge elevation with and without eliminating the mixing effect.

No.	H_0, m	f, %	δD_C, ‰	δD_B, ‰	δD_A, ‰	$H_{R\text{-}A}$, m	$H_{R\text{-}C}$, m
S2	3330	74.5	−64.94	−56.27	−96.04	3694	4456
S5	3335	78.6	−64.35	−56.27	−93.32	3676	4386
S6	3328	75.6	−64.34	−56.27	−93.28	3669	4378
S7	3343	75.9	−64.70	−56.27	−94.93	3697	4439

The results obtained from the application of Equation (4) reveal that, after accounting for the influence of cold-water mixing, the recharge elevation of geothermal water ranges between 3669 and 3694 m (Table 3). Similarly, the recharge elevation of hot water, which mitigates the impact of cold-water mixing, is determined to fall within the range of 4378 to 4456 m. The study area's topography, which exhibits higher elevations in the northwest and lower elevations in the southeast, further supports these findings. Specifically, the primary recharge location for underground hot water is situated in a high mountainous area in the northeast at an elevation of 4300–4500 m, aligning closely with our calculated results.

3.5. Geothermal Heat Reservoir Temperature

Reservoir temperature is widely recognized as a fundamental indicator of geothermal system properties and is a critical factor in assessing geothermal resource potential [30,31]. Common geochemical temperature estimation methods include the Na-K, Na-K-Ca, K-Mg, and SiO_2 temperature scales, among others [32]. These approaches primarily rely on chemical reactions between groundwater and the surrounding rock under varying temperature conditions to infer the heat storage temperature [21]. However, in hot-water areas, underground hot water mixes with significant quantities of shallow circulating cold water during its upwelling to the surface. This extensive mixing can disrupt the chemical equilibrium established by deep geothermal water to varying degrees. Notably, prior research in this area is limited, with no previous investigations into geothermal resources in this region. Therefore, before calculating thermal reservoir temperatures, it is essential to conduct a prior assessment of the water–rock equilibrium state. This analysis will enable the selection of a suitable geothermometer for the study area, ensuring accurate and reliable temperature evaluations.

The results of the Na-K-Mg triangulation analysis, as shown in Figure 5, clearly indicate that the geothermal water in the study area falls within the immature zone. This finding underscores the unsuitability of using cationic thermometers for calculating the heat storage temperature in this region.

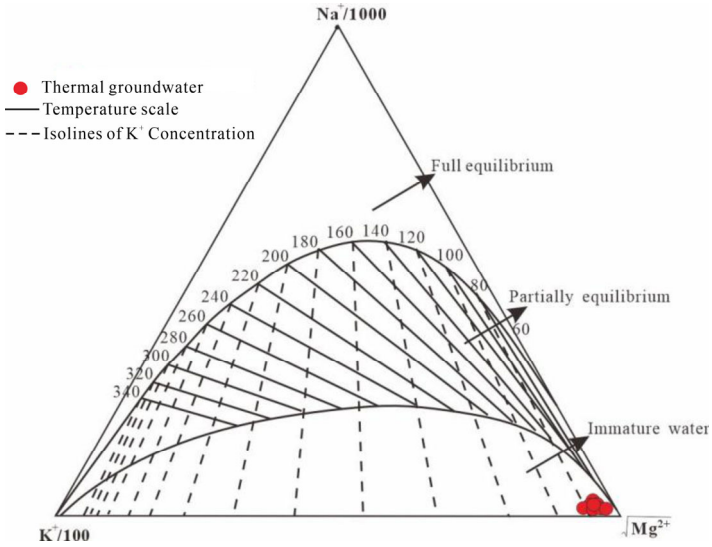

Figure 5. Na-K-Mg triangle diagram of underground hot water in the study area. The base image is from Giggenbach (1988) [33].

The substantial disparity in solubility between hot and cold waters, coupled with SiO_2's resistance to mineral dissolution and re-equilibration during water temperature changes, has established SiO_2 as a prominent indicator of heat storage temperature in underground geothermal systems [29,34]. In its natural state, SiO_2 primarily exists in mineral forms such as quartz, chalcedony, α-cristobalite, β-cristobalite, and amorphous SiO_2. Consequently, an assessment can be made regarding the dissolved forms of various SiO_2 minerals present in geothermal water and their suitability as geothermometers within the study area.

The relationship diagram correlating SiO_2 and $\log(K^2/Mg)$ was utilized to evaluate the dissolution behavior of various SiO_2-containing minerals [35]. As shown in Figure 6, the hot-water samples in this study area are positioned between the chalcedony and quartz curves, indicating that the SiO_2 in hot water primarily results from the dissolution of quartz and chalcedony. Therefore, when calculating the heat storage temperature in this region, it is more appropriate to use the temperature scale derived from quartz and chalcedony.

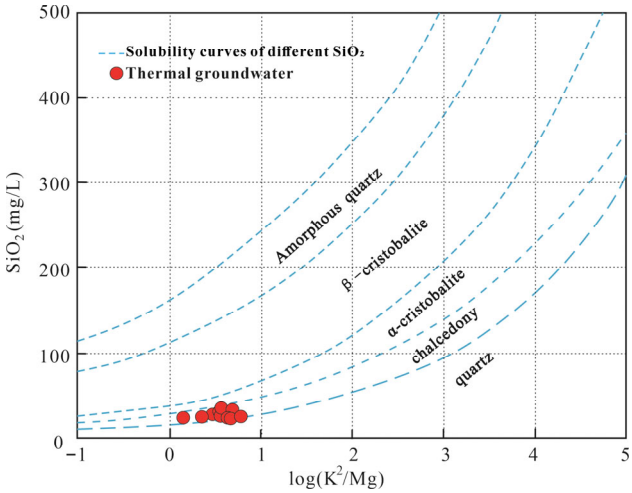

Figure 6. Discrimination diagram for the dissolution of SiO_2 minerals. The lines represent simultaneous attainment of equilibrium for the systems involving silica and K-Mg [35].

The substantial influx of cold water during the upwelling of geothermal water in this region leads to significant challenges in estimating the heat storage temperature based on the measured SiO_2 content of the outcropping hot water [29]. To address this issue, this study employed a binary mixing model (Equation (5)) to inversely calculate the SiO_2 content of the hot water during the mixing process (Table 4). This approach effectively mitigates the impact of mixing on the accuracy of heat storage temperature estimation.

Table 4. Data statistics for the estimation of the geothermal water reservoir temperature in the study area.

Sample NO.	Exposure Temperature, °C	Geothermal Water SiO_2, mg·L^{-1}	Hot and Cold Water Ratio, %	Corrected SiO_2, mg·L^{-1}	Geothermal Reservoir Temperature, °C				Silicon Enthalpy Equation for Geothermal Reservoir Temperature, °C
					Synergistic Impact		Neutralize Combined Interactions		
					Quartz	Chalcedony	Quartz	Chalcedony	
S1	35	40.02	85.6	272.9	91	61	202	184	187
S2	46	39.59	74.5	152.3	91	60	162	138	150
S5	42	37.79	78.60	172.9	89	58	170	147	154
S6	44	39.50	75.60	158.8	91	60	164	141	150
S7	43	39.15	75.90	159.3	90	60	165	141	151
S10	40	39.26	81.60	208.93	90	60	183	162	172

The calculated results (Table 4) indicate that, based on the quartz temperature scale (Equation (6)) without considering mixing effects, the thermal storage temperature of the geothermal system in the hot-water area ranges from 89 to 91 °C. Similarly, using the chalcedony temperature scale (Equation (7)) yields a temperature range of 58 to 61 °C. After accounting for mixing effects, these temperature ranges increase significantly to 162–202 °C for the quartz scale and 138–184 °C for the chalcedony scale. Additionally, the heat storage temperature derived from the silicon enthalpy equation is estimated to be between 150 and 187 °C.

Notably, without considering mixing effects, the temperature values obtained from both the quartz and chalcedony scales are substantially lower compared to those calculated after accounting for mixing effects. Furthermore, the chalcedony temperature scale consistently yields lower values overall. However, the results from the quartz temperature scale align closely with those obtained using the silicon enthalpy equation once mixing effects are considered.

Considering both methods—the quartz temperature scale and the silicon enthalpy equation—the optimal estimated temperatures for the underground hot water reservoir fall within a range of 150 to 202.

Nevertheless, it must be clearly pointed out that the aforementioned assessment is primarily based on inferences drawn from regional geological conditions and surface observations. Currently, there is a lack of direct geochemical evidence regarding microscale silica precipitation phenomena within boreholes or deep fractures. Consequently, the temperature estimation method employed in this study carries a certain degree of uncertainty. If localized silica precipitation exists along the deep circulation pathways that have not been detected by our investigation, it may result in an underestimation of the deep SiO_2 concentration calculated from spring orifice samples, thereby potentially leading to a certain degree of underestimation in the estimated thermal reservoir temperature. This potential error represents an inherent limitation of the model used in this research. Future studies could

further constrain and reduce such uncertainty by collecting fluid samples from different depths for geochemical modeling or by cross-validating with other geothermometers.

3.6. Circulation Depth of Geothermal Water

The calculated circulation depth of underground hot water in the study area, determined using Equation (8), ranges from 3211 to 4292 m. This indicates significant subsurface hydrothermal fluid flow within the region.

The radioactive isotope tritium is widely used for determining the age of groundwater. In this study, the tritium concentrations in the primary geothermal water were measured and are presented in Table 5. The results indicate relatively low tritium levels in the geothermal water, ranging from 0.9 ± 0.6 to 1.6 ± 0.7 TU. These tritium-poor characteristics suggest that the underground hot water in the study area originates from a deep-cycling system that predates 1952 and has limited recycling and renewal capacity [26]. Furthermore, carbon dating reveals an apparent age of 35.02 ± 1.76 ka, which corroborates these findings. This age indicates that the underground hot water in the region is composed of deep-circulating "ancient water," further supporting the conclusion that it is part of a long-residence-time geothermal reservoir.

Table 5. ^{3}H and ^{14}C test results for geothermal water in the study area.

No.	^{3}H/TU	Modern Carbon Percent/%	Apparent Age/ka
S1	1.2 ± 0.5	Unmeasured	Unmeasured
S2	1.4 ± 0.6	Unmeasured	unmeasured
S5	1.3 ± 0.6	Unmeasured	Unmeasured
S6	1.5 ± 0.6	Unmeasured	Unmeasured
S7	0.9 ± 0.6	1.45 ± 0.31	35.02 ± 1.76
S10	1.6 ± 0.7	Unmeasured	unmeasured

3.7. Formation Patterns of Underground Hot Water

The study area is situated at the convergence zone of the Qilianshan island arc belt and the Central Qilian–Huangyuan block. Having undergone multiple phases of tectonic activity since the Paleozoic period, the region exhibits a highly developed fault system. This fault system belongs to the Qin–Qi–Kun fault system within the Paleo-Asian fault regime, a product of the evolution of the Qin–Qi–Kun multi-island ocean. The faults are predominantly densely clustered in bundles. Based on their strike orientation, they can be categorized into two groups: the main set consists of NW–NWW-trending and approximately E–W-trending (partially arcuate) faults, while the secondary set comprises NE–NEE-trending faults. The former constitutes the primary-phase faults, whereas the latter are subordinate faults formed during later stages. These later faults often follow and rework pre-existing ones, with some exhibiting boundary fault characteristics. In terms of their kinematic nature, the faults can be classified as thrust faults, strike-slip faults, normal faults, and faults of an undetermined nature. Collectively, this fault system governs the distribution pattern of the stratigraphic units within the area, dissecting various geological bodies into rock blocks of varying sizes [36,37].

Hot springs in the study area primarily emerge along the margins of the Qinghai Lake depression basin, where the basement rocks are relatively ancient. Integrating regional geophysical and geothermal geological background analyses, this study concludes that the geothermal sources within the area are most consistent with a crustal origin. The localized high reservoir temperatures observed within the fault zones can be primarily explained by the following mechanisms: (1) Concentration of regional background heat flow by deep-penetrating fault systems: The NW-trending deep-seated fault systems, such as the

Reshui–Riyueshan fault system, act as efficient conduits for heat and water transfer. They concentrate the regional background terrestrial heat flow, facilitating the upward transport of deep-seated thermal energy [37,38]. (2) Potential contribution of intra-crustal thermal anomalies: The heat sources for these anomalies include radiogenic heat produced by the decay of crustal radioactive elements (e.g., U, Th, and K), as well as potential intra-crustal low-velocity/high-conductivity layers (often interpreted as partial melts or fluid-rich zones) within the middle-lower crust, as revealed by geophysical surveys. These intra-crustal thermal anomalies can constitute significant local heat sources [37,38].

Although the regional northern Qilian deep-seated fault group is a crust-penetrating structure that could potentially provide a deep pathway for mantle-derived heat contributions, it must be explicitly stated that this study has not obtained direct geophysical or geochemical evidence of the involvement of mantle heat in the local thermal circulation. Therefore, the extent of mantle heat flow contribution currently remains a scientific hypothesis, awaiting verification through future studies employing deep geophysical imaging and analyses of noble gas isotopes, among other methods [37,38]. The compartmentalized compressional–shear structural system within the area has created favorable conditions for the formation, migration, and emergence of geothermal water.

During the Neotectonic period, the study area was controlled by a NE-oriented stress field, causing reactivation of the Reshui–Riyueshan fault zone within the North Central Qilian fault group. This fault zone exhibits good connectivity and strong continuity, accompanied by significant hydrothermal activity. The NE-trending tensile fractures developed in the study area possess excellent water-conducting properties. Their interconnections, compounded with deep-seated faults that primarily facilitate heat conduction (such as the Reshui–Riyueshan fault), provide favorable spaces for the abundant emergence of hot springs at sites with oblique fault intersections. Consequently, the multi-phase active deep-seated fault system serves as the key pathway for the upward transport of deep crustal thermal energy, while the NE-trending tensile fractures constitute the primary pathways for the infiltration of meteoric water and its subsequent deep circulation. The coupled structural control over fluid migration and heat transfer plays a dominant role in the formation of therapeutic hot springs in this region [36].

The geothermal system in the Reshui coalfield area of Gangcha County is a typical fault-controlled, banded medium-low-temperature geothermal system. Its formation and distribution are closely related to the regional tectonics around Qinghai Lake and the development of carbonate rocks. The interconnected and compounded structural framework within the area provides superior conditions for the formation, migration, and emergence of geothermal water. The carbonate rock strata of the Jixianian Kesuer Formation (Jxk) provide favorable reservoir space for the geothermal system; the overlying slate member (Jxkss), composed of silty slate interbedded with sandstone, constitutes an effective aquitard and caprock; the underlying limestone member (Jxkls), consisting of dolomite and limestone, forms a good thermal reservoir. These lithological characteristics, combined with the interconnected tectonic features, establish the foundation for hydrothermal storage and migration within the geothermal system. Furthermore, the relatively abundant precipitation resulting from the local microclimate around Qinghai Lake, along with the development of weathering fractures in the bedrock, provides favorable recharge conditions for the geothermal system.

Based on comprehensive research integrating the geological structure, hydrogeology, geothermal geology, and hydrochemical/isotopic characteristics of the study area, a conceptual model for the formation of the geothermal water system in the Gangcha Reshui area has been constructed (Figure 7). Recharge to the system primarily originates from atmospheric precipitation in the high-altitude mountainous area (4300–4500 m) to the north-

east. After infiltration, groundwater enters the carbonate aquifer of the Jixianian Kesuer Formation (Jxk) and percolates deeper, initiating a deep-circulation process. During deep circulation, the groundwater is primarily heated by the background terrestrial heat flow, which is potentially augmented by the aforementioned intra-crustal thermal anomalies. The estimated deep thermal reservoir temperature ranges between 150.30 °C and 202.16 °C. The overall flow direction of the geothermal water is from the northeast to the southwest, following the regional topography and structural trend. Upward migration occurs along fault conduits at locations where valleys deeply incise the terrain and at fault intersections. During ascent, the deep hydrothermal fluids mix with shallow-circulating cold water from the quaternary system. The high degree of mixing leads to a reduction in the temperature of the emerging hot springs to between 35.6 °C and 46.2 °C.

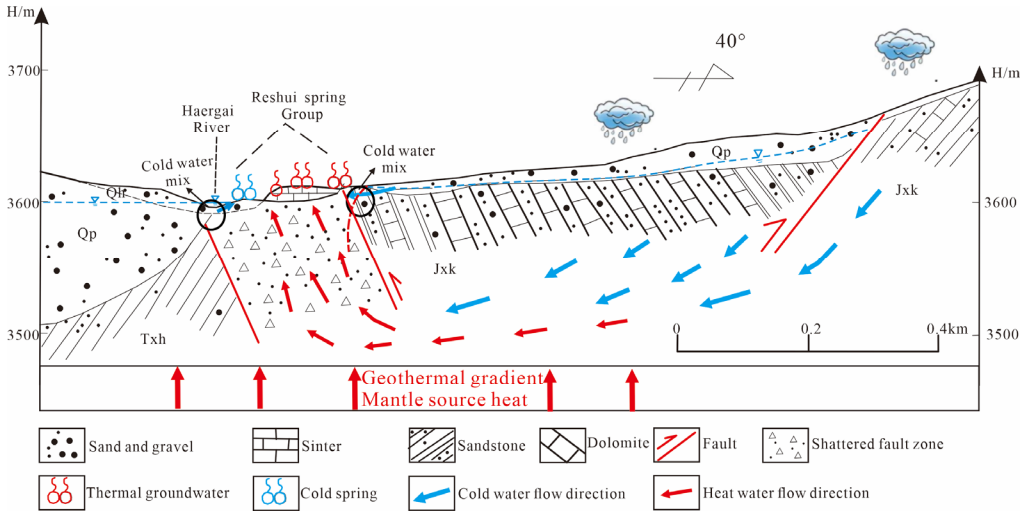

Figure 7. Schematic diagram of the formation mode of the hot-water mineral spring group.

Groundwater flows from the northeast to the southwest, following the regional topography and structural extensions. As it ascends, it follows fault channels within deep, complexly interwoven valleys. During this upwelling process, the groundwater's hot water mixes with shallow quaternary-circulation cold water in the surrounding areas at a mixing ratio ranging from 74.5% to 85.6%. The temperature of the exposed hot water decreases to 35.6–46.2 °C. This integrated model effectively describes the formation and circulation of the underground hot-water system in the Gangcha Hot-Water Area.

4. Conclusions

The study investigates the hydrochemical characteristics and thermal reservoir temperature of a fault-controlled geothermal field in the Northern Qinghai Lake Coalfield Area, providing valuable insights into the system's formation and operational mechanisms. The geothermal water is classified as a low-temperature, weakly acidic to near-neutral HCO_3•Ca•Mg type, with temperatures ranging from 35.6 to 46.2 °C. Stable isotopic analyses reveal distinct signatures for geothermal waters, indicating deeper circulation compared to cold springs and river waters. The silica–enthalpy mixing model shows significant cold-water mixing during upwelling, with mixing ratios between 74.5% and 85.6%. Recharge elevation is estimated to be 4378–4456 m, suggesting a primary recharge zone in the high mountains to the northeast. Geothermometry estimates reservoir temperatures of 150–202 °C, and circulation depths range from 3211 to 4291 m. Low tritium levels and carbon dating indicate a deep-cycling system with "ancient water" predating 1952, characterized by long residence times. The geothermal system's development is closely linked

to regional tectonics, fault systems, and the Kesuer Formation (Jxk) acting as the reservoir. These findings provide a scientific foundation for the development and sustainable use of geothermal resources in the northern Qinghai Lake region and offer insights applicable to analogous fault-controlled geothermal systems across the Qinghai–Tibetan Plateau.

Author Contributions: Conceptualization, Z.Q. and Y.Z.; methodology, Y.Z.; supervision, Z.Q.; investigations, Z.Q., Y.Z., H.W., W.P. and S.H.; formal analysis, B.R., Y.Z., J.Z. and Z.Q.; data curation, Z.Q.; writing—original draft, Y.Z., Z.Q. and B.R.; writing—review and editing, Y.Z., Z.Q., B.R., S.H., J.Z., H.W. and W.P. All authors have read and agreed to the published version of the manuscript.

Funding: This study was financially supported by the Science and Technology Innovation Foundation of Survey Center of Comprehensive Natural Resources (KC20250015) and China's Geological Survey Project (DD20220958).

Data Availability Statement: The data presented in this study are available on request from the corresponding author.

Acknowledgments: All authors thank the anonymous reviewers and editorial staff for their guidance and assistance in improving this manuscript.

Conflicts of Interest: The authors declare no conflicts of interest.

References

1. Soltani, M.; Moradi Kashkooli, F.; Dehghani-Sanij, A.; Nokhosteen, A.; Ahmadi-Joughi, A.; Gharali, K.; Mahbaz, S.; Dusseault, M. A comprehensive review of geothermal energy evolution and development. *Int. J. Green Energy* **2019**, *16*, 971–1009. [CrossRef]
2. Zhang, H.-S.; Feng, Q.-D.; Zhang, D.-Y.; Zhu, G.-L.; Yang, L. Bacterial community structure in geothermal springs on the northern edge of qinghai-tibet plateau. *Front. Microbiol.* **2023**, *13*, 994179. [CrossRef]
3. Anyim, K.; Gan, Q. Fault zone exploitation in geothermal reservoirs: Production optimization, permeability evolution and induced seismicity. *Adv. Geo-Energy Res.* **2020**, *4*, 1–12. [CrossRef]
4. Gao, H.; Wang, J.; Yang, Y.; Pan, X.; Ding, Y.; Duan, Z. Permafrost hydrology of the qinghai-tibet plateau: A review of processes and modeling. *Front. Earth Sci.* **2021**, *8*, 576838. [CrossRef]
5. Zhen, Z.; Yu, P.L.; Chen, H.-J.; Luo, H.-F.; Zhao, Y.-F.; Jiang, B. Genetic analysis and resource evaluation of the xining geothermal field in qinghai province. *Geol. China* **2015**, *42*, 803–810.
6. Yuan, F.; Zhang, C.; Sun, S.; Luo, B. Study on spatial relationship between earthquakes and geothermal in qinghai province. *Plateau Earthq. Res.* **2017**, *29*, 1–6.
7. Tang, X.; Wang, G.; Ma, Y.; Zhang, D.; Liu, Z.; Zhao, X.; Cheng, T.-J. Geological model of heat source and accumulation for geothermal anomalies in the gonghe basin, northeastern tibetan plateau. *Acta Geol. Sin.* **2020**, *94*, 2052–2065.
8. Zhang, S.; Wu, H.; Zhang, Y.; Song, J.; Zhang, L.; Xu, W.; Li, D.; Li, S.; Jia, X.; Fu, L. Characteristics of regional and geothermal geology of the reshuiquan hdr in guide county, qinghai province. *Acta Geol. Sin.* **2020**, *94*, 1591–1605.
9. Duo, J. Typical high temperature geothermal system-basic characteristics of yangbajain thermal field. *Eng. Sci.* **2003**, *1*, 42–47.
10. Wang, Y.; Lin, W.; Lu, R.; Zhang, S.; Zhu, J. Terrestrial heat flow and heat controlling factors in the northeastern tibetan plateau: A case study of gonghe basin. *Renew. Energy* **2026**, *256*, 124038. [CrossRef]
11. Long, D.; Zhou, X.; Yang, K.; Gu, P.; Gao, Y.; Wang, S.; Chen, G. Research on relationship between the deep structure and geothermal resource distribution in the northeastern xizang plateau. *Geol. China* **2021**, *48*, 721–731.
12. Liu, L.; Lu, R.; Xie, W.; Liu, B.; Wang, Y.; Yao, H.; Lin, W. Distribution and hydrogeochemical characteristics of hot springs in northeastern tibetan plateau. *Earth Sci. Front.* **2024**, *31*, 173–195.
13. Hu, S.; Huang, S.; He, L.; Pang, Z.; Wang, J. Lithospheric thermal structure and geothermal resource potential in chinese mainland. *Act Geol. Sin.* **2013**, *87*, 36.
14. Liu, J.; Shi, J.; Yao, X.; Li, Q.; Chang, Z. The control of neo-tectonic activity over geothermal resource in the taxkorgan basin on the northeastern margin of the pamir. *Geol. China* **2018**, *45*, 681–692.
15. Zhang, Y.; Xiao, Y.; Yang, H.; Wang, S.; Wang, L.; Qi, Z.; Han, J.; Hao, Q.; Hu, W.; Wang, J. Hydrogeochemical and isotopic insights into the genesis and mixing behaviors of geothermal water in a faults-controlled geothermal field on tibetan plateau. *J. Clean. Prod.* **2024**, *442*, 140980. [CrossRef]
16. Zhang, X. *1:1,000,000 Geological Map and Instructions of Qinghai Province*; Qinghai Geological Survey Institute: Qinghai, China, 2005.
17. Feng, Y.; He, S. Basic characteristics of tectonics inthe qilian mountains and itsneighbouringson genetic environments of early paleozoicmarine volcanics. *Northwest Geol.* **1995**, *16*, 92–103.

18. Tolstikhin, I. Determination of groundwater age by the t-^ 3he method. *Geochem. Int.* **1969**, *6*, 810–811.
19. Mahlknecht, J.; Hernández-Antonio, A.; Eastoe, C.J.; Tamez-Meléndez, C.; Ledesma-Ruiz, R.; Ramos-Leal, J.A.; Ornelas-Soto, N. Understanding the dynamics and contamination of an urban aquifer system using groundwater age (14c, 3h, cfcs) and chemistry. *Hydrol. Process.* **2017**, *31*, 2365–2380. [CrossRef]
20. Fournier, R.O.; Truesdell, A. Geochemical indicators of subsurface temperature: Part 2, estimation of temperature and fraction of hot water mixed with cold water. *J. Res. US Geol. Surv.* **1974**, *2*, 263–270.
21. Lang, X.; Lin, W.; Liu, Z.; Xing, L.; Wang, G. Hydrochemical characteristics of geothermal water in guide basin. *Earth Sci.* **2016**, *41*, 1723–1734.
22. Gu, W. *Isotope Hydrology*; Science Press: Beijing, China, 2011.
23. Mao, X.; Zhu, D.; Ndikubwimana, I.; He, Y.; Shi, Z. The mechanism of high-salinity thermal groundwater in xinzhou geothermal field, south china: Insight from water chemistry and stable isotopes. *J. Hydrol.* **2021**, *593*, 125889. [CrossRef]
24. Yang, Y. Precipitation and Runoff Process in Shaliu Riverbasin of Qinghai Lake Based on Hydrogen-Oxygenstable Isotope Technique. Master's Thesis, Qinghai Normal University, Xining, China, 2019.
25. Dai, W.; Jiang, X.; Luo, Y.; Zhang, H.; Lei, Y.; Tong, J. Identification and quantification of factors controlling hydrogen and oxygeisotopes of geothermal water: An example from the guide basin, qinghai province. *Earth Sci. Front.* **2021**, *28*, 420–427.
26. Zhou, X.; Jin, X.; Liang, S. *Special Topics on Groundwater Science*; Geological Publishing House: Beijing, China, 2017.
27. Liu, H.; Han, H.; Zhang, L. *Survey and Evaluation Report of Natural Mineral Water for Drinking No.1 Hot Water Mineral Water in Gangcha County, Qinghai Province*; Qinghai Mineral Water Survey and Evaluation Center: Xining, China, 1993.
28. Wu, H.-W.; Li, X.-Y.; Zhao, G.-Q.; Li, G.-Y.; Li, Z.; Li, L. The variation characteristics of δ 18 o and δd in precipitation and river water, qinghai lake basin. *J. Nat. Resour.* **2014**, *29*, 1552–1564.
29. Xiao, Y.; Mo, P.; Zhang, J.; Zhao, X.; Li, J.; Zhang, P.; Li, F. A new viewpoint concerning genesis of karst thermal groundwater under cold-hot water mixing. *J. Eng. Geol.* **2021**, *29*, 383–393.
30. Tian, J.; Pang, Z.; Guo, Q.; Wang, Y.; Li, J.; Huang, T.; Kong, Y. Geochemistry of geothermal fluids with implications on the sources of water and heat recharge to the rekeng high-temperature geothermal system in the eastern himalayan syntax. *Geothermics* **2018**, *74*, 92–105. [CrossRef]
31. Yang, P.; Dan, L.; Groves, C.; Xie, S. Geochemistry and genesis of geothermal well water from a carbonate–evaporite aquifer in chongqing, sw china. *Environ. Earth Sci.* **2019**, *78*, 33. [CrossRef]
32. Abdelali, A.; Nezli, I.E.; Kechiched, R.; Attalah, S.; Benhamida, S.A.; Pang, Z. Geothermometry and geochemistry of groundwater in the continental intercalaire aquifer, southeastern algeria: Insights from cations, silica and so4–h2o isotope geothermometers. *Appl. Geochem.* **2020**, *113*, 104492. [CrossRef]
33. Giggenbach, W.F. Geothermal solute equilibria. Derivation of na-k-mg-ca geoindicators. *Geochim. Cosmochim. Acta* **1988**, *52*, 2749–2765. [CrossRef]
34. Li, X.; Huang, X.; Liao, X.; Zhang, Y. Hydrogeochemical characteristics and conceptual model of the geothermal waters in the xianshuihe fault zone, southwestern china. *Int. J. Environ. Res. Public Health* **2020**, *17*, 500. [CrossRef]
35. Giggenbach, W.; Glover, R. Tectonic regime and major processes governing the chemistry of water and gas discharges from the rotorua geothermal field, new zealand. *Geothermics* **1992**, *21*, 121–140. [CrossRef]
36. Zhang, C.; Li, X.; Ma, F.; Fu, C.; Bai, Z. Formation model of geothermal water in chaya of tibet: Perspective from hydrochemistry and stable isotopes. *Geoscience* **2021**, *35*, 199–208.
37. Guo, J.; Tang, F.; Guan, H.; Zhao, H.; Zhao, X.; Danzeng, G.; Du, B. Structure-thermal coupling model of the high temperature geothermal system in rujiao on the xizang plateau. *Geol. China* **2023**, *50*, 1621–1631.
38. Luo, Z.; Zhou, X.; He, M.; Liang, J.; Li, J.; Dong, J.; Tian, J.; Yan, Y.; Li, Y.; Liu, F. Earthquakes evoked by lower crustal flow: Evidence from hot spring geochemistry in lijiang-xiaojinhe fault. *J. Hydrol.* **2023**, *619*, 129334. [CrossRef]

Disclaimer/Publisher's Note: The statements, opinions and data contained in all publications are solely those of the individual author(s) and contributor(s) and not of MDPI and/or the editor(s). MDPI and/or the editor(s) disclaim responsibility for any injury to people or property resulting from any ideas, methods, instructions or products referred to in the content.